

Published in final edited form as:

Phys Med Biol. 2010 September 7; 55(17): 4977–4992. doi:10.1088/0031-9155/55/17/007.

A feasibility study using radiochromic films for fast neutron 2D passive dosimetry

Samuel L Brady¹, Rathnayaka Gunasingha², Terry T Yoshizumi^{2,3,4,7}, Calvin R Howell^{5,6}, Alexander S Crowell^{5,6}, Brent Fallin^{1,6}, Anton P Tonchev^{5,6}, and Mark W Dewhurst⁴

¹ Medical Physics Graduate Program, Duke University, Durham, NC 27705, USA

² Radiation Safety Division, Duke University, Durham, NC 27705, USA

³ Department of Radiology, Duke University Medical Center, Durham, NC 27710, USA

⁴ Department of Radiation Oncology, Duke University Medical Center, Durham, NC 27710, USA

⁵ Department of Physics, Duke University, Durham, NC 27706, USA

⁶ Triangle Universities Nuclear Laboratory, Duke University, Durham, NC 27706, USA

Abstract

The objective of this paper is threefold: (1) to establish sensitivity of XRQA and EBT radiochromic films to fast neutron exposure; (2) to develop a film response to radiation dose calibration curve and (3) to investigate a two-dimensional (2D) film dosimetry technique for use in establishing an experimental setup for a radiobiological irradiation of mice and to assess the dose to the mice in this setup. The films were exposed to a 10 MeV neutron beam via the $^2\text{H}(d,n)^3\text{He}$ reaction. The XRQA film response was a factor of 1.39 greater than EBT film response to the 10 MeV neutron beam when exposed to a neutron dose of 165 cGy. A film response-to-soft tissue dose calibration function was established over a range of 0–10 Gy and had a goodness of fit of 0.9926 with the calibration data. The 2D film dosimetry technique estimated the neutron dose to the mice by measuring the dose using a mouse phantom and by placing a piece of film on the exterior of the experimental mouse setup. The film results were benchmarked using Monte Carlo and aluminum (Al) foil activation measurements. The radiochromic film, Monte Carlo and Al foil dose measurements were strongly correlated, and the film within the mouse phantom agreed to better than 7% of the externally mounted films. These results demonstrated the potential application of radiochromic films for passive 2D neutron dosimetry.

1. Introduction

A report in 2001 (Bazioglou and Kalef-Ezra 2001) demonstrated the potential for slow and fast neutron dosimetry using radiochromic film. Since that time, radiochromic film has seen innovative changes in structure, material and sensitivity (Fuss *et al* 2007, Gorny *et al* 2005, Soares 2006). The purpose of this work is to investigate the feasibility of using modern radiochromic film as a passive neutron dosimeter for two-dimensional (2D) neutron dosimetry. Current neutron dosimetry techniques can be performed using single-point measurements; two examples of these techniques are direct ion chamber dose measurements and indirect neutron fluence-to-dose measurements using activation foils. However, 2D neutron dosimetry comparison is mostly restricted to time-consuming Monte Carlo simulations. On the other hand, film dosimetry offers a potential passive measurement

technique that exploits simultaneous multi-point direct dose measurements for quick experimental setup and target dose analysis. The film dosimetry technique can be fully analyzed within a few hours to a day after exposing the film; thus, giving the film the advantage for quicker 2D neutron comparison than Monte Carlo simulations.

Two types of modern radiochromic film were chosen for analysis in this neutron film study. Both films have a number of features that make them attractive for use in neutron dosimetry, which are: both film types have a high-spatial resolution; a large fractional composition of hydrogen (ISP 2007, Lewis 2008); they are insensitive to visible light (ISP 2007, Rampado *et al* 2006) and minor temperature changes (Rink *et al* 2008), which make it convenient for them to be used in a normal laboratory environment; they are water resistant, thereby allowing the films to be submerged in a water bath (ISP 2007, vanBattum *et al* 2008) for use in direct dosimetry measurements in an imitation soft tissue environment and they are mechanically pliable, allowing them to be shaped to the surface of the object being studied.

In this work (1) the sensitivity to 10 MeV neutrons was experimentally determined for two types of modern radiochromic films, (2) a technique for relating radiation dose to the film optical density (OD) was developed and (3) a novel 2D film neutron dosimetry technique was investigated for use in establishing an experimental setup for a radiobiological irradiation of mice and to assess the dose to the mice in this setup.

2. Materials and methods

2.1. Radiochromic film and digitization process

XRQA and EBT radiochromic films (both films, International Specialty Products, Wayne, NJ) were investigated as 2D neutron dosimeters. Differences in the two films' construction are shown in figure 1. XRQA, shown in figure 1(A), measured approximately 0.3 mm thick, had an average weighted density of 1.44 g cm^{-3} and an atomic composition (Lewis 2008) of H—47.5%, C—34.4%, O—13.6%, N—3.2%, Br—0.5%, Cs—0.5%, Li—0.2%, Ba—0.2%, S—0.2% and Cl—0.1% for an effective atomic number of (Z_{eff}) (McCullough and Holmes 1985) 24.95. EBT, shown in figure 1(B), also measured approximately 0.3 mm thick, had an average weighted density of 1.38 g cm^{-3} and atomic composition (ISP 2007) of C—42.3%, H—39.7%, O—16.2%, N—1.1%, Li—0.3% and Cl—0.3% for a Z_{eff} of 6.96. The radiochromic films, unlike radiographic films, did not require chemical post-processing for image formation and data analysis; instead, they underwent a solid-state polymerization reaction to the incident ionizing particles (Rink *et al* 2005b). The polymerization reaction created a polymer dye complex that appeared darker in color to the eye compared to unexposed portions of the film; the reaction occurred in real time. After the radiation source was shut off the polymerization reaction required time to polymerize before film digitization could be made. In the case of these experiments, the films were allowed 24 h for the polymerization reaction to induce negligibly small increases in netOD.

Commercial flatbed scanners have been investigated for use as radiochromic film digitization devices (Alva *et al* 2002, Devic *et al* 2005, 2009, Ferreira *et al* 2009, Paelinck *et al* 2007, Saur and Frengen 2008). In this work, XRQA and EBT films were digitized using an EPSON Expression 10000XL commercial flatbed scanner. The EPSON scanner was capable of transmission and reflection densitometry. The XRQA film was digitized using reflection densitometry (Thomas *et al* 2003, Alva *et al* 2002) necessitated by the film's opaque white polyester film layer, see figure 1(A), and EBT film was digitized using transmission densitometry. The scanner employed a xenon gas fluorescent source light and a linear charged coupled device (CCD) array (Ferreira *et al* 2009) for film readout. The scanner's source light illuminated only during previewing and scanning; so to 'warm-up' the scanner, ten blank scans were performed in succession and then discarded. Warming up the

scanner provided a more stable light source with time and more consistent OD readings (Paelinck *et al* 2007). The films were placed on the scanner in an area of high source-light uniformity, which corresponded to the center of the scanner. Each film was scanned five times (Paelinck *et al* 2007) at a resolution of 72 pixels per inch (0.4 mm pixels), with no color corrections, and saved in uncompressed Tagged Image File Format. All films were digitized using 48-bit color depth with RGB file format (16-bit per color channel). The red (R of the RGB) channel was extracted for analysis in Matlab (R2007a, Mathworks, Natick, MA) since radiochromic film readout sensitivity has been shown to be optimized using a red light due to the films reported absorption spectrum maximum at 635 nm (Devic *et al* 2007). The final image consisted of an average of the five scans using a 3×3 pixel kernel. The films were scanned prior to irradiation and then carefully realigned on the scanner bed for post-irradiation scans (alignment error measured to be ~ 1 mm). Once irradiated, the films darkened such that their OD exponentially grew with exposure (Cheung *et al* 2005, Rampado *et al* 2006, Rink *et al* 2005a). A net OD (netOD) (Devic *et al* 2005) was calculated as the log transformation of the ratio of pre-irradiation (I_{pre}) to post-irradiation (I_{post}) scanner light intensity values:

$$\text{netOD} = \text{OD}_{\text{post}} - \text{OD}_{\text{pre}} = \log_{10} \left(\frac{I_0}{I_{\text{post}}} \right) - \log_{10} \left(\frac{I_0}{I_{\text{pre}}} \right) = \log_{10} \left(\frac{I_{\text{pre}}}{I_{\text{post}}} \right). \quad (1)$$

2.2. Neutron beam production

Film exposure to fast neutrons was studied at the Triangle Universities Nuclear Laboratory (TUNL) at Duke University. The neutron beam was produced via the $^2\text{H}(d,n)^3\text{He}$ reaction, by bombarding a pressurized deuterium gas cell (7.8 atm), see figure 2, with a deuteron beam from the Tandem Van de Graaff accelerator (Hutcheson *et al* 2007, Pedroni 1986, Swartz 2007). The subsequent neutron beam had a monoenergetic peak of 10 MeV with a full width at half maximum (FWHM) of 1 MeV (at 7.8 atm), and a continuum of low energy neutrons due to the break-up of the incident deuteron beam (a major peak at 2.7 MeV) and the deuterium gas threshold (a major peak at 4.4 MeV). The spectrum of low energy neutrons accounted for only $\sim 5\%$ deuteron breakup, and $\sim 1\%$ deuterium threshold, of the overall beam flux along the central axis of the neutron beam compared to the major flux peak at 10 MeV; the break-up neutrons contributed even lesser to the overall neutron beam when measured 10° from the main beam axis (Swartz 2007). The cross section of the $^2\text{H}(d,n)^3\text{He}$ reaction was sharply forward-angle peaked due to the forward momentum of the deuteron beam incident on the deuterium gas cell. The neutrons were emitted in a conical geometry, centered on the beam axis, with angular distributions with respect to energy. The kinematics of the reaction was such that the most energetic neutrons were emitted at 0° , along the central beam axis, and the energies of the emitted neutrons decreased with increasing angle, e.g., the neutron energies decreased by $\sim 10\%$ (to 9 MeV) with a conical diameter of 20 cm when considering a 17 cm distance from the center of the 6 cm gas cell to the front of the film and mouse setups (Swartz 2007).

2.3. Radiochromic film sensitivity to fast neutrons

XRQA and EBT films' sensitivity to a 10 MeV neutron beam was tested. The radiochromic films were mounted on a Plexiglas board (3 mm thick) and placed 17 cm away from the neutron source. One XRQA film was mounted on the front side (closest to the neutron source) of the Plexiglas board, and one EBT film was mounted on the backside of the board. The films and board were set perpendicular to the main axis of the neutron beam and were exposed simultaneously. Films were digitized and then imported into Matlab for analysis. Both films were spatially registered and line profiles were taken from each film type. Film sensitivities were investigated by comparing FWHM measurements of the two line profiles,

and by comparing max netOD values at the center of the measured neutron dose distribution for each film type.

2.4. Radiochromic film netOD-to-dose calibration

A netOD-to-soft tissue dose calibration technique was established using the following experimental setup. A water bottle (6 cm length and 2.7 cm diameter) was mounted inside a box and the films were arranged at different distances with respect to the water bottle. Six XRQA films were exposed to three different neutron exposures. Each neutron exposure provided a different flux density and film distance configuration to vary film netOD values and neutron doses. Two aluminum (^{27}Al) foils (1.3 cm diameter and 0.03 cm thickness) were placed at the front and backsides of the water target to estimate the neutron flux from Al foil activation ($^{27}\text{Al}(n,\alpha)^{24}\text{Na}$) where the alpha particle reaction creates a ^{24}Na atom that de-excites by a 1368 keV γ -ray). Film and foil exposures were generally performed simultaneously. A film exposure configuration is shown in figure 3.

After each neutron irradiation, the films were digitized and film pixel values were converted to netOD using equation (1). The netOD used in the calibration curve analysis was the mean value of a region of interest (ROI) that measured ~ 1.3 cm in diameter and was taken from the center of the neutron OD distribution on the films. The dose used in the calibration curve analysis was considered for soft tissue and calculated using the FLUKA2008 (Fasso *et al* 2003) Monte Carlo code. To calculate the neutron dose to a soft tissue target in the Monte Carlo simulations, the film material was replaced by A-150 material, a soft tissue equivalent plastic. The accuracy of the Monte Carlo calculations was verified by comparing the neutron dose to the water in the bottle (D_{water}), as calculated from Monte Carlo simulations and that to D_{water} determined from the neutron flux measured by Al foil activation spectroscopy. Monte Carlo simulations determined D_{water} over the entire volume of water within the bottle; however, the average D_{water} at the surface of the water bottle (i.e. the entrance dose) was compared with the Al foil dose results. The Al foil was located within ~ 1 mm of the front of the bottle of water, see figures 3(A) and (B). After irradiation, the neutron-induced activity of the Al foil was measured off-line in TUNL's low-background counting area. Each of the neutron-activated Al foils was measured using a high purity germanium (HPGe) detector (Canberra, Meriden, CT) to determine the neutron flux at the location of each foil. An energy window for the γ -ray spectroscopy was set at 1368 keV with an energy resolution of 1.8 keV FWHM. The $^{27}\text{Al}(n,\alpha)^{24}\text{Na}$ has an activation threshold of 3249 keV neutrons. Though, the neutron alpha threshold does allow for some deuterium breakup low energy neutrons to interact in the Al foil, the cross section of interaction is near zero for neutron energies < 6 MeV (0.001 barns) compared to neutron energies of 10 MeV (0.089 barns) (Perey *et al* 1972). Hence the measured neutron flux from ^{24}Na atom de-excitation by 1368 keV γ -ray was a measurement of the 10 MeV neutrons and not the lower energy neutron contamination. The majority of the measurement error from the HPGe detectors was determined to be detector efficiency for the 1368 keV γ -rays. The systemic error was measured to be $\sim \pm 5\%$ of measurement with an additional $\pm(1-2)\%$ being purely due to statistical uncertainty.

From the Al foil flux density measurements, D_{water} was then calculated using the following relation:

$$D_{\text{water}} (\text{cGy}) = \phi_n \cdot F_{\text{water}}^{10 \text{ MeV}}, \quad (2)$$

where ϕ_n was the measured neutron flux and $F_{\text{water}}^{10 \text{ MeV}}$ was the neutron kerma factor for 10 MeV neutrons obtained from the ICRU Report 26 (ICRP 1977).

2.5. 2D film dosimetry technique

As part of a small animal neutron dosimetry project, radiochromic films were used to measure the dose distribution of the neutron beam for each target setup and to estimate the dose to mice. The small animal dosimetry project utilized a hollow Plexiglas box (12.5 cm wide \times 25.3 cm tall \times 8 cm deep) that was constructed to hold seven 50 ml vials with one center hole and six peripheral holes each offset by 4.0 cm (measured center-to-center from central to peripheral slots), shown in figure 4(A). The front of the Plexiglas box was positioned 17 cm away from the neutron source so that the peripheral holes were elevated 13° from the central neutron axis. The energy of the neutrons at 13° from the central axis was measured to have had $E_n > 9.72$ MeV, or within 2.8% of the 10 MeV neutrons along the 0° axis (Swartz 2007). The mice were held within the 50 ml vials during the neutron irradiation. The Plexiglas box and 50 ml vials were attached 17 cm above a rotation stage, shown in figure 4(B). The rotation stage was used to rotate the mice 180° half way through the irradiation to provide a more uniform exposure over the full length of each mouse; the neutron radiation was terminated while the stage rotated 180°, and was re-engaged once the mice and film were in position.

2.5.1. Immersed film measurements—To measure the dose over the full length of the mouse volume, a 6 cm long (4.5 cm without the cap) \times 2.7 cm diameter polyethylene bottle was filled with water and used to emulate a mouse target. XRQA film was cut to fit within the bottle and immersed in the water along the central-long axis of the bottle. The water-filled bottle and film were then placed within a 50 ml vial, see figure 4(A). One vial was placed at the center position of the Plexiglas box and another vial was placed at the 3 O'clock peripheral position; the center position of the Plexiglas box was aligned to the central axis of the neutron beam. Once positioned, the films within the bottle were exposed to half the calculated run time. The resulting longitudinal dose profile of the irradiated film was numerically 'rotated' 180° and added to the original dose profile to generate an estimated dose to mouse volume to simulate the 180° rotation exposure pattern that the real mice underwent. Even though XRQA films have polyester layers that protect the radiosensitive active layers in the film (figure 1), the sides of the film are not sealed and therefore water penetrated into the film from the edges. XRQA films were immersed in water for about 3 h. The rate of water penetration (~ 7 pixels h^{-1}) necessitated measurements to be 0.7 cm (~ 20 pixels), from the edge of the films.

2.5.2. Externally mounted film measurements—Six mice were placed within 50 ml vials and loaded onto the rotation stage in the six peripheral slots. XRQA films were placed on the front (cap) and backside (tip) of the 50 ml vials, see figure 4(C). The films were used to estimate the entrance dose to the mice. Additionally, two Al foils were placed on top of the 50 ml vial caps (directly behind the film), and on the tips of the vials (directly in front of the film) for an independent measurement of the neutron flux incident on the mice. One set of Al foils was placed at 3 O'clock and the other set at 9 O'clock. The mice were rotated 180° half way through the irradiation for improved uniform exposure. The films were rotated along with the mice. The overall exposure time was 1.95 h.

2.5.3. Analysis—Immersed film dose measurements were compared to externally mounted film dose measurements as a means to verify the accuracy of the external mounted film measured dose. The accuracy of the film in water was compared to independent Monte Carlo-calculated doses over the length of the water bottle, and the accuracy of the externally mounted films was independently compared to Al foils located on the 50 ml vials.

3. Results

3.1. Radiochromic film's sensitivity to neutron exposure

Neutron fluence distribution was measured using XRQA and EBT as shown in figures 5(A) and (B). FWHM and netOD values for each film type were calculated from line profiles, see figure 5(C), taken along similarly positioned dotted lines represented in figure 5(B). The measured FWHM of the netOD distribution of each film type was: $\text{FWHM}_{\text{XRQA}} = 9.5$ cm and $\text{FWHM}_{\text{EBT}} = 9.6$ cm. netOD measurements of the two film types showed that XRQA film ($\text{netOD}_{\text{XRQA}}$ measured 0.255) had a 39% greater sensitivity to 10 MeV neutrons than EBT film ($\text{netOD}_{\text{EBT}}$ measured 0.156) when exposed to a dose level of 165 cGy.

3.2. Film calibration technique

For the dose calibration technique, the highest neutron flux measured using the activation foil technique was $(8.5 \times 10^6 \text{ } 6.9 \times 10^4) \text{ n cm}^{-2} \text{ s}^{-1}$ at the front of the water bottle. Using equation (2) and $F_{\text{water}}^{10 \text{ MeV}}$ from ICRU data tables, the calculated dose rate to the water target, from the location of the foil, was $(189.0 \pm 9.5) \text{ cGy h}^{-1}$ and the calculated dose rate to the front of the water target from the Monte Carlo calculation was $(188.3 \pm 0.001) \text{ cGy h}^{-1}$, an agreement to better than 0.4%. Additionally, the dose rate measured from the foil placed behind the water bottle was $(44.3 \pm 2.3) \text{ cGy h}^{-1}$ as compared with the Monte Carlo calculation of $(38.3 \pm 0.01) \text{ cGy h}^{-1}$, an agreement to better than 14%. The Al foil, compared with the Monte Carlo calculation at the rear of the water bottle, was located ~ 2 cm from the water bottle; this may allow for a possible explanation of the larger discrepancy in Al foil and Monte Carlo dose rate comparison at the rear of the water bottle. Having established the accuracy of the Monte Carlo calculations, the dose to soft tissue used for the calibration data was simulated using Monte Carlo with the results shown in table 1, and plotted versus measured film netOD values in figure 6.

3.3. 2D film dosimetry technique

3.3.1. Immersed film dose measurements—Dose distributions and central axis dose profiles for films placed in water bottles located in the center slot and a peripheral slot are shown in figures 7(A)–(D), respectively. The entrance dose to the center film measured 190.6 cGy, and the dose at the entrance on the periphery film was 88.1 cGy. When the longitudinal dose profile was combined with the 180° rotated duplicate to create an estimation of the overall dose to the targets, the doses to the center film were 247.0 cGy at the entrance and exit and a minimum of 192.1 cGy at the center of the film. The overall change in dose along the length of the center filmstrip was 55.0 cGy. The doses to the combined peripheral profiles were 123.2 cGy at the entrance and exit and a minimum of 115.9 cGy at the center of the film. The overall change in dose along the length of the peripheral filmstrip was 7.3 cGy. A Monte Carlo calculation of the dose response of the film in the peripheral water target was compared to the measured film dose, see figure 8. A correlation calculation of the two profiles was performed as a means of quantitatively assessing the similarity in the Monte Carlo calculated and film responses. The correlation coefficient for curves in figure 8 was 0.9982.

3.3.2. Externally mounted film dose measurements—XRQA film was placed on each end of the mouse holder. The cap side film was closer to the neutron source than the mice during the first half of the mouse exposure, see figure 9(A). The second film was placed on the tip side of the mouse holder and finished closer to the neutron source than the mice during the second half of the mouse exposure, see figure 9(B). Orthogonal line profiles show symmetrical dose responses in the vertical and horizontal directions, see figures 9(C) and (D). The dose profiles in figure 9(C) did not overlap as well as the dose profiles in

figure 9(D) because the film was not centered horizontally on the neutron beam axis. Thus, when the mouse stage and film were rotated the film was offset slightly causing a shift in the horizontal line profile. The offset of the film is also manifested by the elongation of the central dose distribution in figure 9(A), which measured an artificially increased central dose along the horizontal line profile in figure 9(C) around the 7 to 9 cm point as compared to figure 9(D). The cap and tip side film responses were averaged to give a measured dose of (114.4 ± 2.6) cGy, whereas the average Al foil response was 159.3 cGy with ± 3.4 cGy statistical error and ± 8 cGy (~5%) systemic error from the HPGe γ -ray spectroscopy.

3.3.3. Immersed film measurement compared to externally mounted

measurement—The combined externally mounted film dose responses was (114.4 ± 2.6) cGy, and the measured dose in the film placed at the peripheral slot within the water target was 123.2 cGy. The results for the externally mounted film agreed to better than 7% of the estimated mouse dose from the measurements with film in water, where the later method was assumed to be more accurate.

4. Discussion

The discrepancy in the doses at the peripheral location determined by the external film and Al foil methods is attributed mainly to a systematic feature in the neutron foil activation technique. The film and foil dose values were measured at similar locations off the main neutron beam axis. However, in the neutron activation measurements the Al foil was treated as a point source in calculating the flux from the counts in the γ -ray energy spectrum measured with the HPGe detector. As an indirect point dose dosimetry system, Al foils were incapable of measuring the effects of the dose gradient at the peripheral location. The XRQA film dose response, at the peripheral locations of the external mounted films, measured an average difference in dose rate response from the foils of 28%. The deviation in value quoted for the XRQA film was due to the averaging of the values in areas of steep dose gradient. The dose gradient was a result of the rapid fall off of the neutron beam intensity moving away from the 0° axis. The external XRQA films did agree with the average Al foil response when comparing the average maximum dose instead of the mean. The average maximum dose value from the cap and tip side films was 156.5 cGy, which had an agreement of better than 2% with the similarly located Al foils.

The XRQA film measured a greater sensitivity to neutron irradiation than EBT film. The greater sensitivity to neutron-induced signal is assumed to come from the greater density of hydrogen in the XRQA film (48%) compared to the EBT film (40%) and the larger effective Z of the XRQA film ($Z_{\text{eff}} = 24.95$) compared with EBT film ($Z_{\text{eff}} = 6.96$). The larger Z_{eff} results in more efficient ionization of the recoil protons in the XRQA film. Hydrogenous material is known to be the most effective at absorbing energy from fast neutrons with the ${}^1_0\text{H} + {}^1_0\text{n} \rightarrow {}^1_1\text{H} + {}^0_1\text{n}$ elastic scattering reaction. A hydrogen detector provides the greatest cross section for elastic scattering of incident neutrons thereby better preserving directional information from the initial fast neutrons along the main beam axis and providing the most accurate neutron distribution mapping as compared to carbon target interactions (XRQA-34%, EBT-42%). Due to the greater sensitivity to neutron dosimetry, XRQA film was used in the development of the film calibration technique and the dosimetry method for the mouse irradiation experiments.

Radiochromic films were developed to be sensitive to photon radiation, and therefore the signal readout from the films exposed to a mixed neutron and γ -ray field will be a measurement of neutron and γ -ray dose. The extent of the γ -ray contribution to film response signal was analyzed. The neutron beam comprised three distinct types of radiation:

fast 10 MeV mono-energetic neutrons from the ${}^2\text{H}(d,n){}^3\text{He}$ reaction, continuous energy neutrons from the breakup of deuterons in beam and in the deuterium gas cell and γ -rays (Swartz 2007). Additionally, γ -ray contribution to the overall radiation field consisted of three parts: (1) neutron capture on hydrogen (${}^1\text{H}(n,\gamma){}^2\text{H}$ reaction) in the targets and the radiation shielding material; (2) de-excitation of excited nuclei in the beam stop (gold) and beam collimation apertures (tantalum); and (3) from the Al foil de-excitation by ${}^{24}\text{Na}$ γ -rays.

The breakup neutrons were shown to have a wide spectrum of energies from ~ 1 MeV to ~ 6.5 MeV where the peaks of the measured continuum of flux were centered at 2.7 MeV and 4.4 MeV. The breakup flux was measured along the main axis of the neutron beam and measured $\sim 6\%$ of the monoenergetic neutron contribution, where the break-up neutrons contributed much less to the overall neutron beam when measured 10° from the main beam axis (Swartz 2007).

The γ -ray components were analyzed to determine their impact on the overall film dose. First, the dose component to the XRQA film from the γ -rays emitted from the ${}^1\text{H}(n,\gamma){}^2\text{H}$ reaction was calculated using Monte Carlo. The percent dose contribution from ${}^1\text{H}(n,\gamma){}^2\text{H}$ γ -rays are shown in table 1. The maximum contribution of the ${}^1\text{H}(n,\gamma){}^2\text{H}$ reaction γ -rays to the dose measured by the films was shown to be $<2\%$. Second, the γ -ray contribution from the deuteron beam interactions with the materials in the beam collimation and beam stop materials were measured previously for 8 MeV neutrons. In the previous report (Swartz 2007), the γ -ray and neutron doses were separately measured at the same location along the beam axis and the γ -ray contribution was measured to be 5% of the neutron beam and is assumed to be approximately similar for 10 MeV neutrons. Third, the γ -ray dose contribution from Al foil activation, through ${}^{24}\text{Na}$ de-excitation by γ -ray, was shown to have a negligible impact on measured film dose response. Dose profiles in figure 9 demonstrated similar dose responses when taken from the films through regions where Al foils overlapped, and would have exposed the films with γ -rays, and through regions where Al foils were not present to expose the films with γ -rays. The contamination of a purely neutron measured signal in the film due to γ -rays was minimal compared to the measured neutron doses for several different conditions. Overall, γ -ray and breakup neutron contamination accounted for $\sim 13\%$ of the total dose to the films along the central beam axis, but only $\sim 3\%$ when measured 10° off the central beam axis (Swartz 2007), the position where the mice were exposed.

The XRQA films were also exposed to scattered neutrons and γ -rays. The geometrical isotropy of the γ -rays and the scattered neutrons possibly contributed to a consistent baseline dose measured by the film. This baseline dose was evident from the overall exposure of the film in spite of the well-collimated neutron beam. The tails of the dose profile in figure 9 approached a value of ~ 50 cGy when measured outside of the region of direct neutron beam involvement.

Future investigations into neutron detection using radiochromic film should include an investigation into the possibility of changing XRQA and EBT film sensitivities with changes in dose levels, and the dosimetric effects, as a function of changing neutron energies, for a better understanding of the dose to the film as a function of neutron energy falloff away from the 0° main axis.

5. Conclusion

Two types of modern radiochromic film, XRQA and EBT film, were studied as potential 2D neutron dosimeters. XRQA film measured a greater sensitivity to neutron dose than EBT

film by a factor of 1.39 when exposed to a neutron dose of 165 cGy. A netOD-to-dose calibration curve technique was presented. Monte Carlo simulations were used to calculate soft tissue dose to film for 10 MeV neutrons over a range of 0–10 Gy. The Monte Carlo and XRQA film responses were fit using a least-squares fit of a nonlinear function that measured a correlation of 0.9926 with the calibration data. Monte Carlo results were benchmarked against an Al foil activation technique with the results matching within 0.4%. XRQA films were employed to measure a 2D dose distribution of the neutron beam flux for an experimental setup and used to make dose measurements on mouse targets. XRQA films placed in front of the experimental setup and within a bottle of water, to emulate a mouse target, agreed within 7%. The good agreement of the external film with that of the *in vitro* film measurement demonstrated the ability of XRQA film to be used in an uncomplicated passive manner to measure dose by placing a piece of film in front of a target. The XRQA film measurements within the water bottle were compared to the results from Monte Carlo simulations to test the accuracy of the film in neutron dosimetry measurements. The comparison of the film and Monte Carlo responses gave a correlation of 0.9982. To this end, we have demonstrated the potential application of modern radiochromic film for accurate fast neutron dosimetry.

Acknowledgments

This research was, in part, supported by National Institute of Allergy and Infectious Diseases grant 5U19 AI067798-03, by the US Department of Energy Office of High Energy and Nuclear Physics grant DE-FG02-97ER41033, and NIH grant NIBIB T32 EB007185.

References

- Alva H, Mercado-Uribe H, Rodriguez-Villafuerte M, Brandan ME. The use of a reflective scanner to study radiochromic film response. *Phys. Med. Biol.* 2002; 47:2925–33. [PubMed: 12222856]
- Bazioglou M, Kalef-Ezra J. Dosimetry with radiochromic films: a document scanner technique, neutron response, applications. *Appl. Radiat. Isot.* 2001; 55:339–45. [PubMed: 11515658]
- Cheung T, Butson MJ, Yu PK. Post-irradiation colouration of Gafchromic EBT radiochromic film. *Phys. Med. Biol.* 2005; 50:N281–5. [PubMed: 16204869]
- Devic S, Seuntjens J, Sham E, Podgorsak EB, Schmidlein CR, Kirov AS, Soares CG. Precise radiochromic film dosimetry using a flat-bed document scanner. *Med. Phys.* 2005; 32:2245–53. [PubMed: 16121579]
- Devic S, Tomic N, Pang Z, Seuntjens J, Podgorsak EB, Soares CG. Absorption spectroscopy of EBT model Gafchromic film. *Med. Phys.* 2007; 34:112–8. [PubMed: 17278496]
- Devic S, Tomic N, Soares CG, Podgorsak EB. Optimizing the dynamic range extension of a radiochromic film dosimetry system. *Med. Phys.* 2009; 36:429–37. [PubMed: 19291981]
- Fasso A, et al. The FLUKA code: present applications and future developments. High Energy and Nuclear Physics Conf. (La Jolla, CA, USA). 2003 arXiv:physics/0306162v1.
- Ferreira BC, Lopes MC, Capela M. Evaluation of an Epson flatbed scanner to read Gafchromic EBT films for radiation dosimetry. *Phys. Med. Biol.* 2009; 54:1073–85. [PubMed: 19168937]
- Fuss M, Sturtewagen E, Wagter CD, Georg D. Dosimetric characterization of Gafchromic EBT film and its implication on film dosimetry quality assurance. *Phys. Med. Biol.* 2007; 52:4211–25. [PubMed: 17664604]
- Gorny KR, Leitzen SL, Bruesewitz MR, Kofler JM, Hangiandreou NJ, McCollough CH. The calibration of experimental self-developing Gafchromic(R) HXR film for the measurement of radiation dose in computed tomography. *Med. Phys.* 2005; 32:1010–6. [PubMed: 15895584]
- Hutcheson A, et al. Pulsed and monoenergetic beams for neutron cross-section measurements using activation and scattering techniques at Triangle Universities Nuclear Laboratory. *Nucl. Instrum. Methods Phys. Res. B.* 2007; 261:369–72.
- ICRP. *Report 26*. ICRU; Bethesda, MD: 1977. Neutron dosimetry for biology medicine.

- ISP. Gafchromic EBT self-developing film for radiotherapy dosimetry Unpublished (white paper). 2007.
- Lewis, DF. International specialty products, personal communication. 2008.
- McCullough EC, Holmes TW. Acceptance testing computerized radiation therapy treatment planning systems: direct utilization of CT scan data. *Med. Phys.* 1985; 12:237–42. [PubMed: 4000085]
- Paelinck L, De Neve W, De Wagter C. Precautions and strategies in using a commercial flatbed scanner for radiochromic film dosimetry. *Phys. Med. Biol.* 2007; 52:231–42. [PubMed: 17183138]
- Pedroni, RS. PhD Dissertation. Duke University; Durham, NC, USA: 1986. Cross sections and analyzing powers in the 8- to 17-MeV range for neutron scattering from [Fe-54,56], [Ni-58,60], and [Sn-120].
- Perey, FG.; Love, TA.; Kenney, WE. ORNL-4823, ENDF-178. Oak Ridge National Laboratory; Oak Ridge, TN: 1972. A test of neutron total cross section evaluations from 0.2 eV to 20 MeV for C, O, Al, Si, Fe and SiO₂.
- Rampado O, Garelli E, Deagostini S, Ropolo R. Dose and energy dependence of response of Gafchromic(R) XR-QA film for kilovoltage x-ray beams. *Phys. Med. Biol.* 2006; 51:2871–81. [PubMed: 16723772]
- Rink A, Lewis DF, Varma S, Vitkin IA, Jaffray DA. Temperature and hydration effects on absorbance spectra and radiation sensitivity of a radiochromic medium. *Med. Phys.* 2008; 35:4545–55. [PubMed: 18975701]
- Rink A, Vitkin IA, Jaffray DA. Characterization and real-time optical measurements of the ionizing radiation dose response for a new radiochromic medium. *Med. Phys.* 2005a; 32:2510–6. [PubMed: 16193781]
- Rink A, Vitkin IA, Jaffray DA. Suitability of radiochromic medium for real-time optical measurements of ionizing radiation dose. *Med. Phys.* 2005b; 32:1140–55. [PubMed: 15895598]
- Saur S, Frengen J. Gafchromic EBT film dosimetry with flatbed CCD scanner: A novel background correction method and full dose uncertainty analysis. *Med. Phys.* 2008; 35:3094–101. [PubMed: 18697534]
- Soares CG. New developments in radiochromic film dosimetry. *Radiat. Prot. Dosim.* 2006; 120:100–6.
- Swartz, B. MS Thesis. Duke University; Durham, NC, USA: 2007. Characterization of neutron beams produced using the 2H(d,n) reaction for determining dose to small animals.
- Thomas G, Chu RYL, Rabe F. A study of Gafchromic XR type R film response with reflective-type densitometers and economical flatbed scanners. *J. Appl. Clin. Med. Phys.* 2003; 4:307–14. [PubMed: 14604420]
- vanBattum LJ, Hoffmans D, Piersma H, Heukelom S. Accurate dosimetry with Gafchromic EBT film of a 6 MV photon beam in water: what level is achievable? *Med. Phys.* 2008; 35:704–16. [PubMed: 18383692]

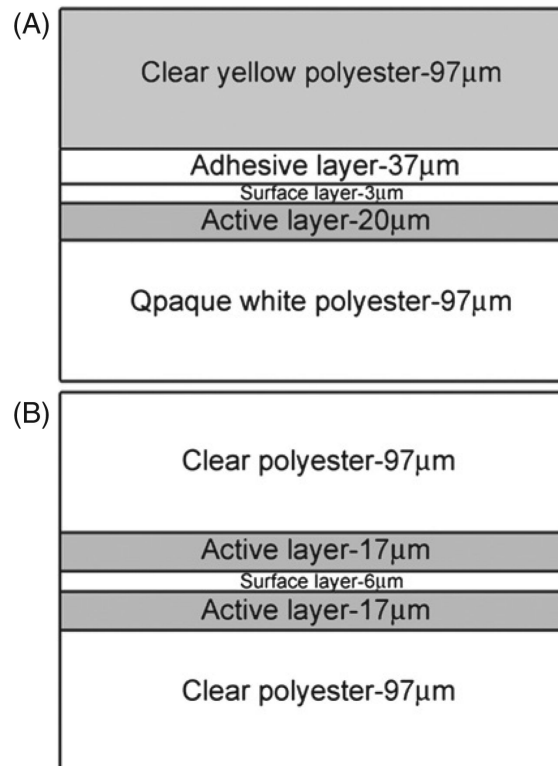


Figure 1.

The diagram represents a cross-sectional view of the XRQA (A) and EBT (B) film structure. The crystalline matrix of radiosensitive monomers is polymerized when exposed to ionizing radiation in the active layer. The polyester layers create a sealed layer to protect the active layer structure from abrasions due to normal handling of the film.

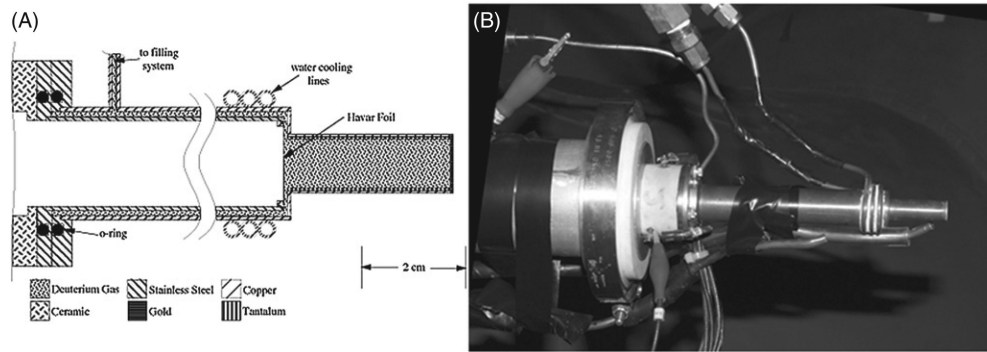


Figure 2.

Gas cell for neutron production is shown. Side cut-away view is provided by Pedroni (1986) (A). The gas cell is constructed of copper with an inner layer of tantalum used to shield copper from a deuteron beam (B). The deuteron beam enters the gas cell from the beam line under vacuum and passes through a thin ($6.4 \mu\text{m}$) Havar foil (used to contain deuterium gas in cell under pressure) and stops in a 0.5 mm thick gold disk. The deuteron beam is collimated upstream of the gas cell to a diameter of 4.8 mm. The cell is water cooled with additional cooling provided by air lines that are directed on the Havar foil and gold disk. The maximum beam current allowed on the gas cell is $\sim 3.0 \mu\text{A}$.

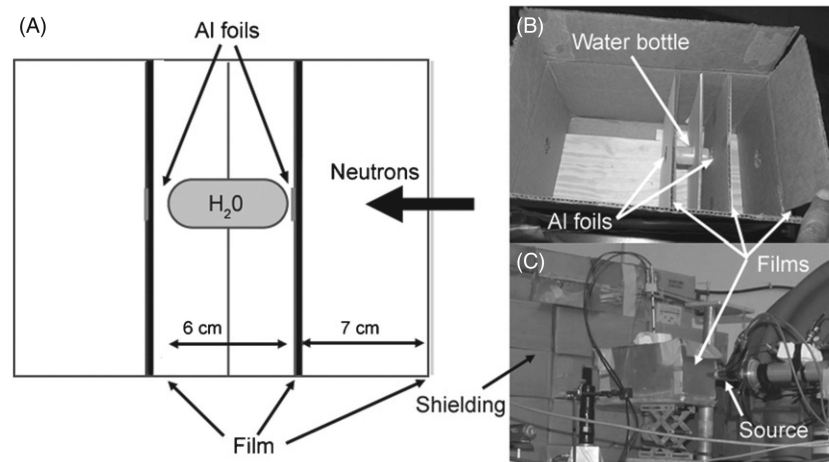


Figure 3. Diagram of a cross-sectional view of the calibration setup is shown in (A). A film and Al foil was placed in the neutron beam path on each end of the water bottle. Additionally, a piece of film was placed on the outside front of the target box. Three separate runs provided six data points. Each run consisted of a film and activation foil irradiation. The inside of the box that held the target (water bottle) and film is shown in (B), and the relative placement of the box with respect to the neutron source with a film placed on the outside is shown in (C).

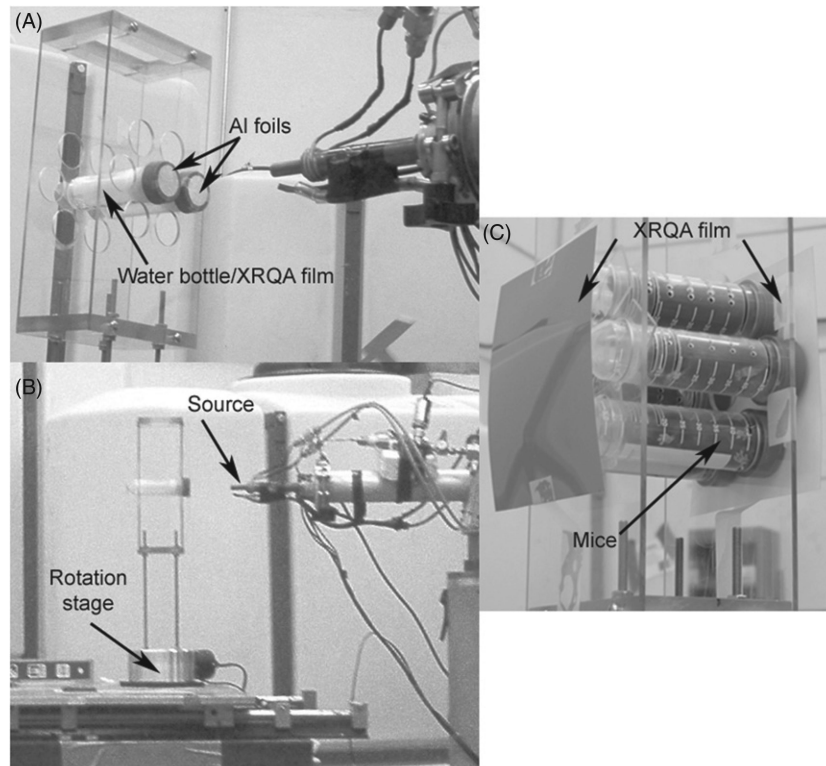


Figure 4. XRQA film was immersed in a water target, used to emulate mice, and loaded inside two 50 ml vials and placed on a Plexiglas box (A). The Plexiglas box and 50 ml vials were mounted on a rotation stage and placed 17 cm in front of the neutron source (B). Six mice were loaded onto the rotation stage with XRQA films placed in front and behind the vials and used for estimating the dose to each mouse; additionally, Al foils were placed on the cap and tip side of the vials containing mice (not visible) as a means to verify measured film doses (C).

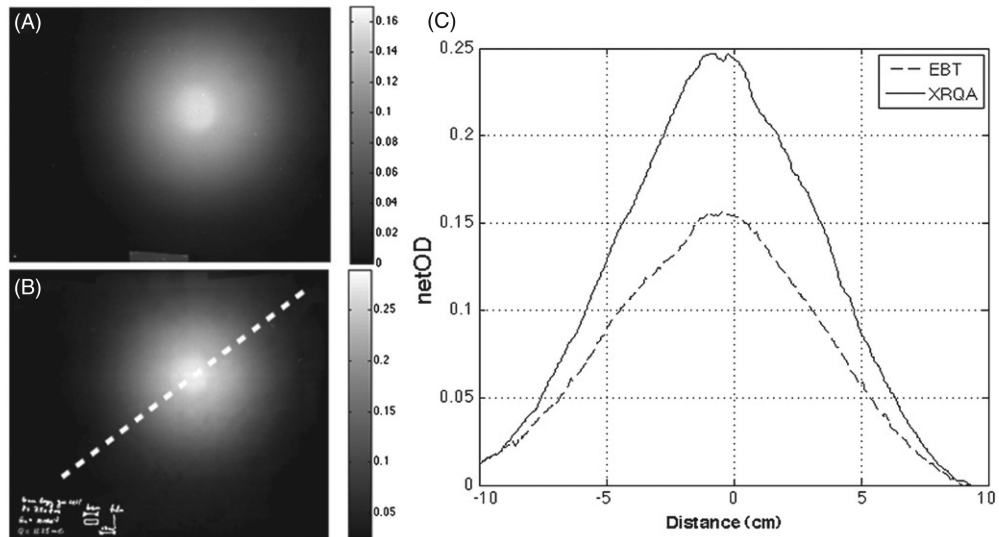


Figure 5. Intensity distribution of the 10 MeV neutron beam measured with EBT film (A) and XRQA film (B). Line profiles taken along dotted line in (B) are plotted for EBT film and XRQA film (C). Both films measured similar FWHM values (~9.5 cm). XRQA film measured a greater sensitivity to 10 MeV neutrons by a factor of 1.39; this is attributed to the larger hydrogen density and higher effective atomic mass of XRQA film than EBT film.

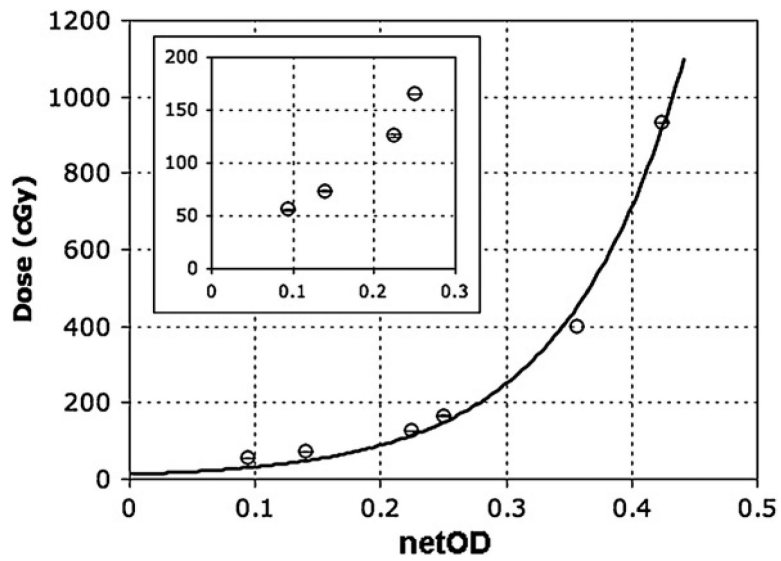


Figure 6. The dose to soft tissue simulated by Monte Carlo is plotted as a function of measured film optical density (OD) of the film. A non-linear regression curve was fit to the six data points with a coefficient of determination (R^2) of 0.9926. The inserted graph is a blow-up of data at low doses (0–200 cGy).

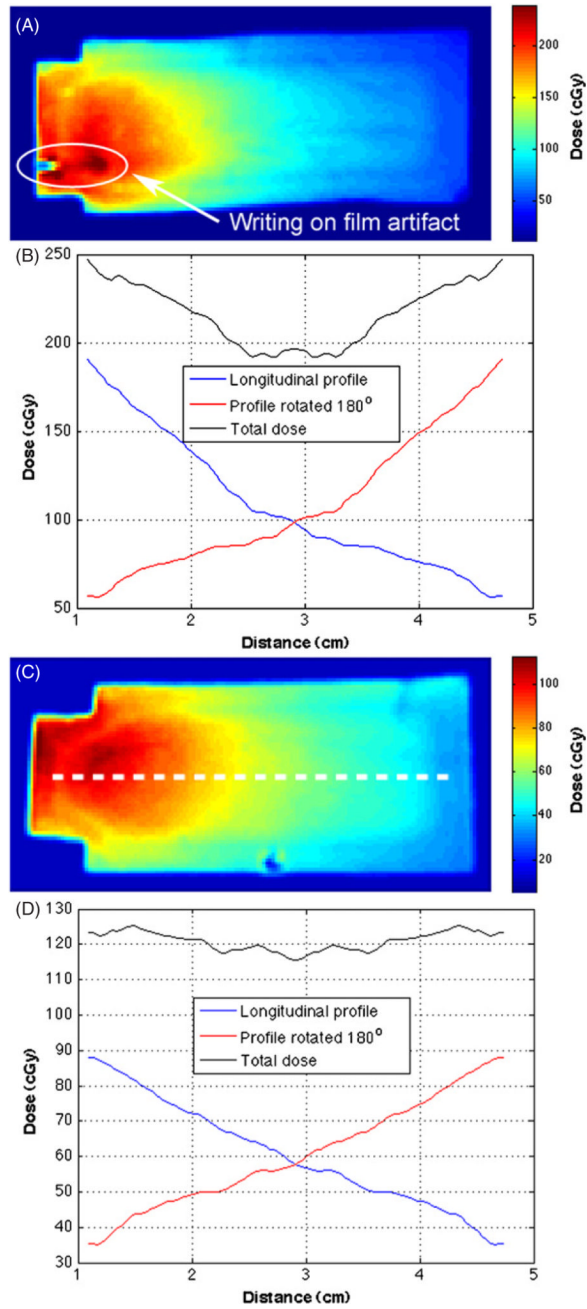


Figure 7. XRQA film inserts were placed along the central-long axis of two water bottles, one centered about the neutron beam (A) and the other placed in a peripheral slot offset 4 cm from the central neutron beam axis (C). Dose profiles, taken along the representative dotted white line (C), provide an estimated total dose to mouse target located at the center (B) and the peripheral (D) mouse locations. The dose to the mouse volume was estimated using a single line profile from film inserts (blue lines) that was rotated 180° (red lines) and added to the original dose profile to create a total dose estimate for film targets (black lines) as if the film were physically rotated 180° as the mice were rotated during the actual irradiation.

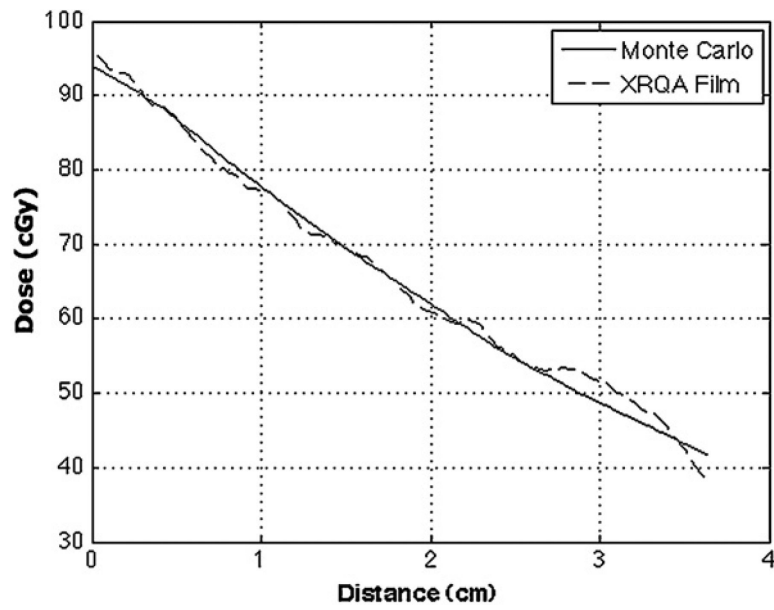


Figure 8. Peripheral XRQA film insert dose response is compared to Monte Carlo calculated dose to peripheral film. Any dose buildup details were not simulated and not shown in the figure. The correlation coefficient for the two plots is 0.9982.

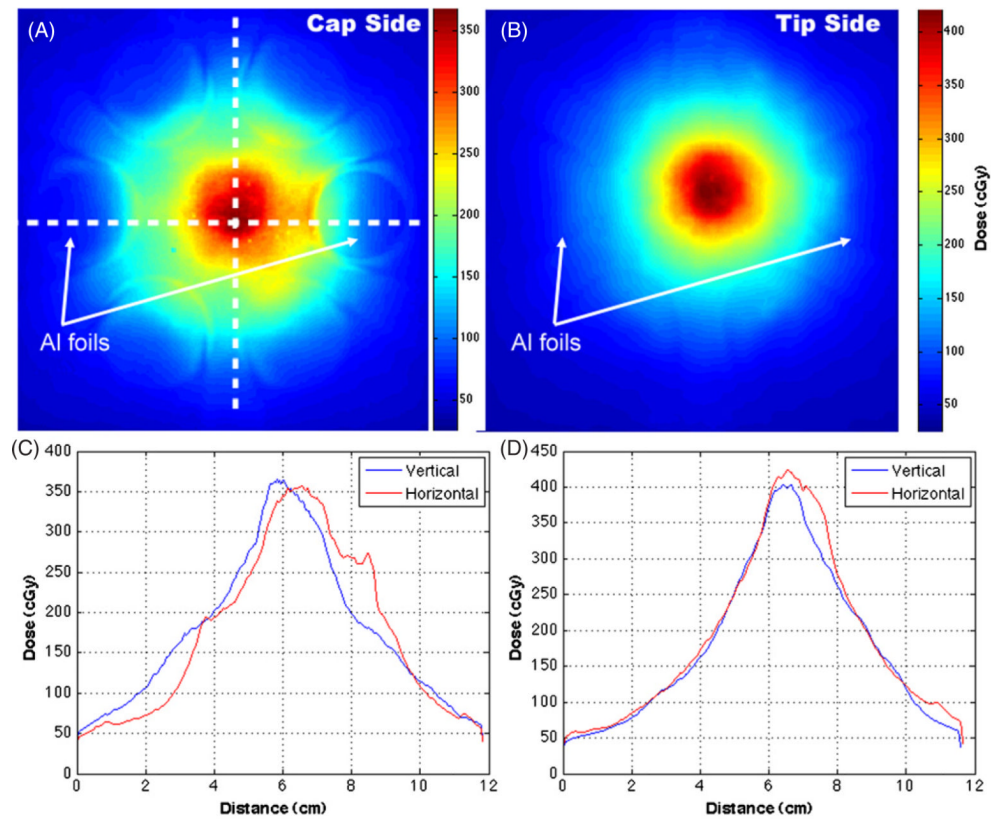


Figure 9.

XRQA film was placed in front and behind of the mouse stage and rotated with the stage. The first film was placed on the ‘cap side’, see figure 4(C), of the mouse stage and was closest to the neutron source for the first half of the mouse exposure (A). The mouse stage and films were then rotated 180°. The second film, placed on the ‘tip side’ of the mouse stage, was exposed closest to the neutron source during the second half of the mouse exposure (B). One set of Al foils was placed on the caps and another set of foils on the tips of the 50 ml vials; one foil located at 3 O'clock and the other at 9 O'clock. γ -ray contamination on a film neutron dose signal due to the Al foil activation de-excitation by ^{24}Na γ -ray emission (1368 keV) was investigated using dose profiles taken from the films through regions where Al foils overlapped, and would have exposed the films with γ -rays, and through regions where Al foils were not present to expose the films with γ -rays (C) and (D).

Table 1

The XRQA film netOD values shown below were averages taken from the center of the exposed films and used along with the total dose calculated by Monte Carlo to generate the calibration curve shown in figure 6. Monte Carlo was used to calculate the total dose to a soft tissue target, which included absorbed doses from neutron and γ -rays. The γ -ray dose quoted below was from the ${}^1\text{H}(n, \gamma){}^2\text{H}$ reaction ($+Q = 2.225$ MeV) simulated by Monte Carlo. The percent dose contribution from γ -rays compared to the total dose is listed. Monte Carlo predicts that the dose contribution from ${}^1\text{H}(n, \gamma){}^2\text{H}$ reaction γ -rays is negligible compared to 10 MeV neutrons.

XRQA film netOD	Monte Carlo		
	Total dose (cGy)	γ -ray dose (cGy)	γ -ray dose contribution (%)
0.095 \pm 0.002	55.66 \pm 0.36	0.18 \pm 0.002	0.3
0.141 \pm 0.002	73.36 \pm 0.03	0.27 \pm 0.001	0.4
0.225 \pm 0.003	125.60 \pm 0.02	0.44 \pm 0.225	0.4
0.251 \pm 0.002	165.24 \pm 0.04	0.82 \pm 0.002	0.5
0.363 \pm 0.003	400.50 \pm 0.15	5.89 \pm 0.012	1.5
0.425 \pm 0.003	930.58 \pm 0.24	13.70 \pm 0.024	1.5